Available online at www.sciencedirect.com
SCIENCE DIRECT®

Journal of the European Ceramic Society 24 (2004) 2407–2416
www.elsevier.com/locate/jeurceramsoc

Fracture behaviour of magnesia and magnesia–spinel composites before and after thermal shock

Cemail Aksel[a,*], Paul D. Warren[b,1], Frank L. Riley[b]

[a]Department of Materials Science and Engineering, Anadolu University, Iki Eylül Campus, Eskisehir 26470, Turkey
[b]Department of Materials, School of Process, Environmental and Materials Engineering, University of Leeds, Leeds LS2 9JT, UK

Received 20 April 2003; received in revised form 18 July 2003; accepted 28 July 2003

Abstract

Microstructural changes, as a consequence of the thermal expansion mismatch between magnesia and spinel phases, and fracture behaviour of magnesia and spinel composites have been investigated as a function of spinel content (10, 20, 30 wt.%). Fracture surfaces of magnesia showed mostly transgranular fracture; for the composites, however, the amount of intergranular fracture increased with increasing spinel content. This change in fracture behaviour is thought to be the main reason for the increase in the work of fracture, γ_{WOF}. The 30% spinel composite was found to exhibit both the greatest resistance to crack propagation, and the greatest resistance to thermal shock damage, with the highest retained strength after quenching.

Keywords: Fracture toughness; $MgAl_2O_4$; MgO; Modulus; Refractories; Strength; Thermal shock; Work of fracture

1. Introduction

Magnesia (MgO) spinel ($MgAl_2O_4$) refractory materials have been used for many years as high strength hot-face refractories, allowing a wide range of compositions and types for a large number of applications to be produced, including rotary cement kilns and steel making vessels.[1–5] MgO–spinel refractories have better resistance to thermal shock and alkali attack compared to other spinels, such as MgO–chrome.[6,7] For environmental reasons, the current trend is to avoid the use of refractories containing chromium oxide, because Cr^{6+} has been associated with allergic skin ulceration and carcinogenic effects in humans.[8] MgO–spinel refractories give significantly (two to three times) longer service lives than conventional MgO–chrome bricks.[4] As a result, MgO–spinel bricks are now preferably used in the cooling zone rather than the upper transition zone of the kiln. In addition, increased use in the sintering zone of cement kilns is providing economic benefits. This new type of MgO–spinel brick can be used in the upper side of the sintering zone of the cement kiln.[9] The life of new type MgO–spinel bricks is longer in the transition and the cooling zone of the rotary cement kiln, as compared to other basic bricks. The stoichiometric type is used in cement kiln linings, and is also used in alumina-based castables especially for ladles. Stoichiometric spinel can also have good resistance to corrosion and erosion.[6]

Spinel particles are added in various proportions to MgO in order to improve thermal shock resistance.[10–12] The reason for these improvements is linked to the large difference in thermal expansion coefficient between MgO ($\sim 13.5\times10^{-6}$ °C^{-1}) and spinel ($\sim 7.6\times10^{-6}$ °C^{-1}).[13,14] During cooling from production temperatures in the region of 1650 °C[15] the difference generates very large hoop tensile stresses around the spinel particles, causing extensive microcracking.[16–18] This leads to greater resistance to the degree of damage from thermal shock.[17,18] Thermal shock behaviour of ceramic materials has been usefully summarised by Green,[19] as described below.

1.1. Thermal shock—fracture initiation

The main thermal shock fracture resistance parameters for a material initially damaged or undamaged, which explains the tendency for cracks to be developed, and therefore loss in strength, can be considered to be

* Corresponding author. Tel.: +90-222-3350580x6355; fax: +90-222-3239501.
E-mail address: caksel@anadolu.edu.tr (C. Aksel).
[1] Now at: Pilkington plc., Group Research, Technology Centre, Hall Lane, Lathom L40 5UF, Lancashire, UK.

0955-2219/$ - see front matter © 2003 Elsevier Ltd. All rights reserved.
doi:10.1016/j.jeurceramsoc.2003.07.005

that for the initiation of fracture caused by thermal stresses:[20,21]

$$R = \frac{\sigma_f(1\text{-}\nu)}{E\alpha};\ R' = \frac{\sigma_f(1-\nu)k}{E\alpha};\ R'' = \frac{\sigma_f(1\text{-}\nu)\phi}{E\alpha} \qquad (1a, b, c)$$

where σ_f is the bend strength, E is Young's modulus, α the mean thermal expansion coefficient, ν Poisson's ratio, k thermal conductivity, and ϕ[19] a stress reduction term. Looking at the parameters R, R' and R'' it is clear that high resistance to fracture initiation can be achieved in materials with high strength and thermal conductivity, and with low values of thermal expansion and Young's modulus. On the contrary, avoiding thermal fracture by increasing strength in order to make initiation difficult is dangerous because once initiated, crack propagation will be fast and catastrophic. This leads to the concept of *damage resistance parameters*.

1.2. Thermal shock—damage resistance parameters

Hasselman approached the problem of thermal shock damage by considering the conditions for relative comparison of the 'degree of damage' on the basis of crack propagation, rather than those for fracture initiation. He derived the following thermal shock damage resistance parameters R''' and R'''', expressing the ability of the material to resist crack propagation and further damage and loss of strength on thermal shocking:[20–22]

$$R''' = \frac{E}{\sigma_f^2}\cdot\frac{1}{(1-\nu)} \text{ and } R'''' = \frac{E}{\sigma_f^2}\cdot\frac{\gamma_{WOF}}{(1-\nu)} \qquad (1d, e)$$

The parameter R'''' can be used to compare the degree of damage of materials with widely different values of γ_{WOF}, such as brittle and ductile materials. The R''' parameter gives information about the minimum in the elastic energy at fracture available for crack propagation, high values indicating an improvement in thermal shock resistance. The criteria for minimising the extent of crack propagation, and for obtaining a low degree of damage,[21] are high values of the Young's modulus, Poisson's ratio, and γ_{WOF} energy, and low strength, provided that there must be some intermediate value of strength and a resulting degree of damage such that the strength (after thermal shock) is a maximum.

1.3. Fracture mechanism of refractories

The fracture mechanism in MgO–spinel refractories relies on the development of microcracks that allow easy crack initiation, but make propagation, in which fracture occurs in a quasi-static manner, more difficult.[15,23–25] When a refractory material is subjected to thermal stresses because of the increase in the temperature gradient, there is no crack propagation and there is no reduction in the strength of a strong material until a critical value is exceed.[26] At a critical temperature (ΔT_c), the surface stress generated will equal the strength and cracks will develop.[25,27] If the same material weakened is thermally shocked through a set of progressively larger temperature differences (above ΔT_c), further crack propagation and strength decrease take place.[25,28] For strong materials, a large amount of elastic energy is available at the fracture-initiation stress, and the crack has a sudden extension, with a large decrease in strength of the material.[24,25,29,30] For weak specimens, which have already had some thermal shock damage, the cracks will propagate in a more controlled manner in response to the variation of the strain with time.[30] In the weakening body containing more microcracks or pores, fracture occurs at a relatively low stress level: rather than fracture occurring catastrophically, the nucleated cracks will propagate only a short distance and will become arrested.[24,25,29,30] Therefore the body retains same strength and will still be useful for many applications.[26,29,31,32] Refractory materials are in general not very resistant to crack initiation, but have a significant resistance to thermal shock damage.[33]

The basic requirements for refractory materials to achieve the highest thermal shock resistance are to obtain the greatest values of either thermal shock parameters or γ_{WOF}/γ_i ratios. It is reported that both thermal shock parameters[23] (R''' and R'''') and γ_{WOF}/γ_i ratios[34] are reliable indicators to determine crack propagation resistance, and can be used to predict the loss in strength of MgO and spinel composites, before thermal shock tests. It is also stated that resistance to thermal shock damage in terms of effect of particle size distribution of spinel particles can be more strongly favoured with materials containing significantly broader distribution of spinel particles, rather than narrow distributed spinel particles, for which a much larger spinel content is required to achieve a similar improvement, on the basis of theoretically calculated thermal shock parameters and experimentally found γ_{WOF}/γ_i ratios.[35]

In this work, the microstructural changes and fracture behaviour of both pure MgO and MgO–spinel composites, as a function of spinel addition, before and after thermal shock testing, have been identified. The relationships between mechanical properties and fracture behaviour of MgO and MgO–spinel composites at high temperatures, depending on volume fraction of spinel, have been reported. The thermal shock resistance of MgO and MgO–spinel composites, as a function of quench temperature, has been investigated. The

optimum spinel content showing the highest resistance to thermal shock has been determined, and the reasons for this are explained to improve the understanding of thermal shock behaviour of MgO–spinel composite materials.

2. Experimental

The basis for the MgO–spinel materials was a nanoparticle size (~30 nm), high surface area, in which MgO powder of >98.0% purity ("light": GPR, BDH, Poole, UK) was calcined at 1300 °C for 2 h to produce a powder with a mean particle size of 0.5 μm. Alcoa MR66 spinel powder (99.5% purity) was air classified to obtain more narrow distributions of median size ~22 μm (Alpine Zig-zag classifier, Augsburg, Germany). Particle sizes were measured by a standard laser scattering method (Mastersizer, Malvern Instruments, Malvern UK). Calcined MgO powder appeared to consist of agglomerates of particles, which were approximately uniform in size, and the average particle size using SEM ranged from 0.3 to 0.4 μm. Spinel powders were very regular in size and shape, compared to MgO, because the use of air classification gave a narrow particle size distribution. The effects of varying the amounts of spinel powder (10, 20, 30 wt.%) were investigated. MgO containing spinel particles reached the theoretical density (~99%), by hot-pressing at ~1720 °C and 20 MPa for 25 min, assuming densities of 3.59 Mg m^{-3} for MgO, and of 3.58 Mg m^{-3} for spinel.[2] Bulk density and apparent porosity were measured using the standard water immersion method.[36] Discs were then cut into bars ~26×3×3 mm^3.

2.1. Strength and Young's modulus measurements

Mechanical measurements of all the spinel composites has been carried out by 3-point bend test, where support roller span was 20 mm, and the cross-head speed was 0.2 mm min^{-1}. The standard equations for the strength[37] (σ_f) and Young's Modulus[38] (E) of a bar are:

$$\sigma_f = \frac{3PL}{2WD^2} \tag{2}$$

$$E = \frac{L^3 m}{4WD^3} \tag{3}$$

where P: load at fracture, L: support span, W: specimen width, D: specimen thickness, and m: slope of the tangent of the initial straight-line portion of the load–deflection curve. Thermal shock tests were made by measuring the strengths of samples that had been subjected to an oil quench of between 200 and 800 °C. Five to ten specimens were normally tested at each temperature to obtain a mean value, using a tensile testing machine (Mayes, SMT50). Modulus values were calculated by drawing a tangent to the steepest initial straight-line portion of the load–deflection curve, where the stiffness of the machine was also considered.[38]

2.2. Fracture toughness and work-of-fracture measurements

Both before and after thermal shock, fracture toughness specimens were cut in the centre of the bar with a 50 μm wide diamond blade to a depth of 0.75 mm, to give a notch depth to thickness ratio (d/D) of 0.25. The standard equations[39–42] for the fracture toughness (K_{1c}) of a notched bar are:

$$K_{IC} = 3Y'PLd^{1/2}/2WD^2 \tag{4a}$$

where

$$Y' = A_O + A_1(d/D) + A_2(d/D)^2 + A_3(d/D)^3 + A_4(d/D)^4 \tag{4b}$$

where d is the notch depth, with $L/D \approx 8$, $A_0 = +1.96$, $A_1 = -2.75$, $A_2 = +13.66$, $A_3 = -23.98$, $A_4 = +25.22$.[42] The plain strain fracture toughness can be defined in terms of materials parameters:

$$K_{IC} = \left(\frac{2E\gamma_i}{1-\nu^2}\right)^{1/2} \tag{4c}$$

where the fracture surface energy (γ_i) is a measure of the resistance to initiation of crack propagation.

Values for the work of fracture (γ_{WOF}) were calculated from load–deflection curves obtained from notched bars deformed in 3-point bend, by measuring the area (U) under the load–deflection curve. γ_{WOF} is given by the following equation:[43,44]

$$\gamma_{WOF} = \frac{U}{2W(D-d)} \tag{5}$$

2.3. Fractography

The CamScan 4 SEM used in this study was equipped with an EDX system for elemental analysis. Secondary electron images were used to examine the size and shape of grains exposed in fracture surfaces; back scattered electron images were used to indicate the presence and position of spinel particles. Grain sizes of polished and thermally etched (1500 °C, 10 min) surfaces were measured from photographs taken in the scanning electron microscope, using a standard line mean intercept method.[45] Unfortunately, fracture origins/shapes were not noted so it is not possible to make definitive statements about crack sizes before and after thermal shock.

[1] Now at: Pilkington plc., Group Research, Technology Centre,

3. Results and discussion

3.1. Microstructure

Fig. 1a–c show the microstructures of the as-processed MgO–spinel composite materials. In general, there was a marked increase in the extent of microcracking with increasing spinel content and also significant changes in the grain size for the different materials. The average grain size of pure MgO was found to be ~32 μm using a standard line intercept method. In composites containing 10% 22 μm spinel, the average MgO grain size increased to ~87 μm, but further addition of spinel reduced the MgO grain size significantly. There was a small amount of microcracking at grain boundaries (intergranular) radiating from spinel particles, which resulted in separation of grain boundaries (Fig. 1a). Composites prepared from 10% spinel powders in general showed a smaller amount of microcracking compared to composites containing higher additions of spinel. In the 20% composites, longer micro-cracks (both transgranular and intergranular) were observed, where the average MgO grain size of this composite was ~50 μm (Fig. 1b). At 30% spinel loading, interlinked transgranular and intergranular radial cracks in the MgO matrix appeared, and the crack length increased significantly (Fig. 1c). The average MgO grain size was ~40 μm.

3.2. Fractography before thermal shock

Fig. 2a–c show fracture surfaces (but not fracture origins) after strength tests of the various materials. Dense MgO (Fig. 2a), hot-pressed, had very fine, usually spherical, pores (~1–3 μm), at the grain boundaries and within the grains. Fracture surfaces showed that there was some intergranular fracture (along the grain boundaries), but the fracture was

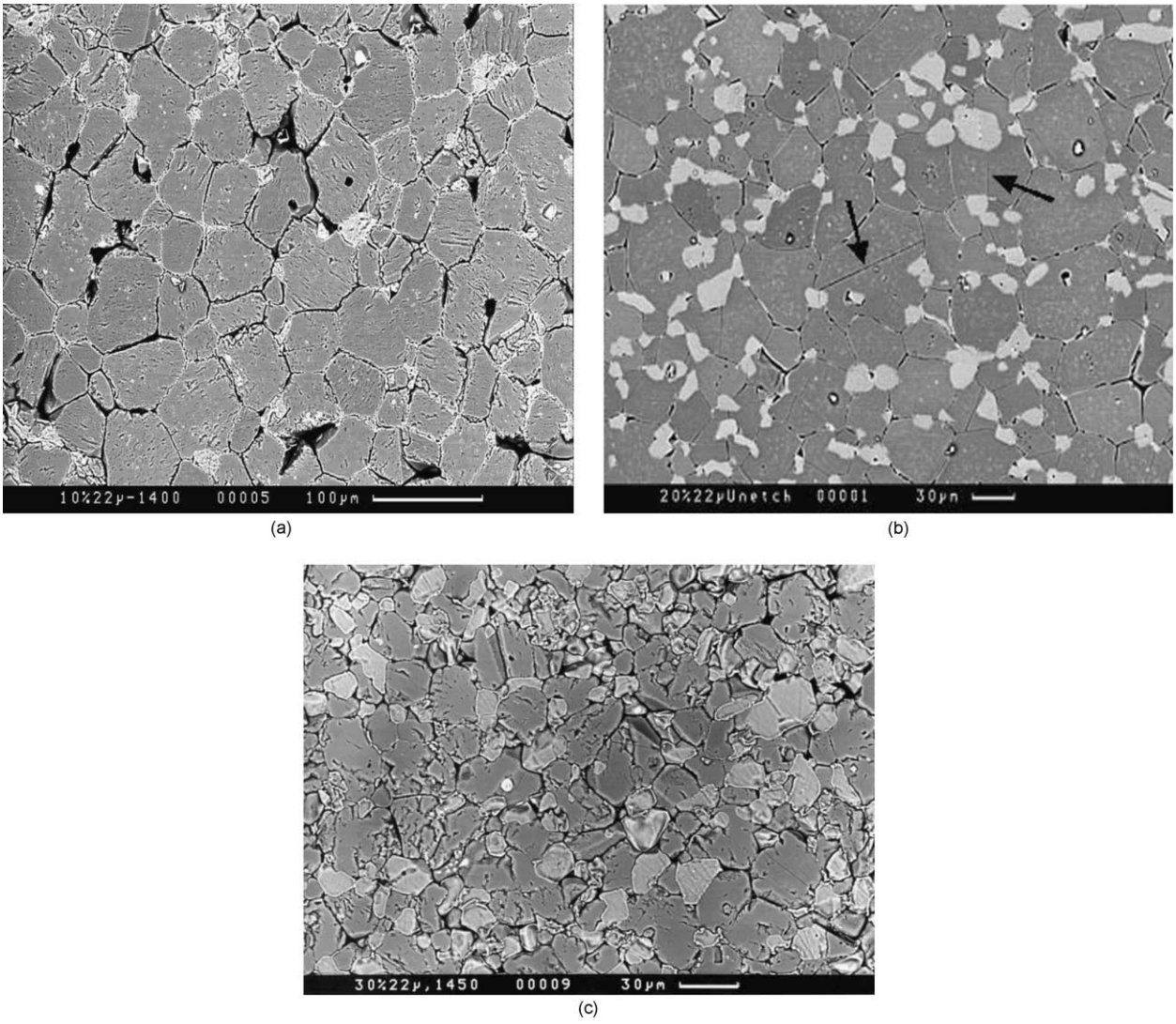

Fig. 1. a–c. Microstructures of (a) 10%-, (b) 20%- and (c) 30%-containing 22 μm spinel–magnesia composites.

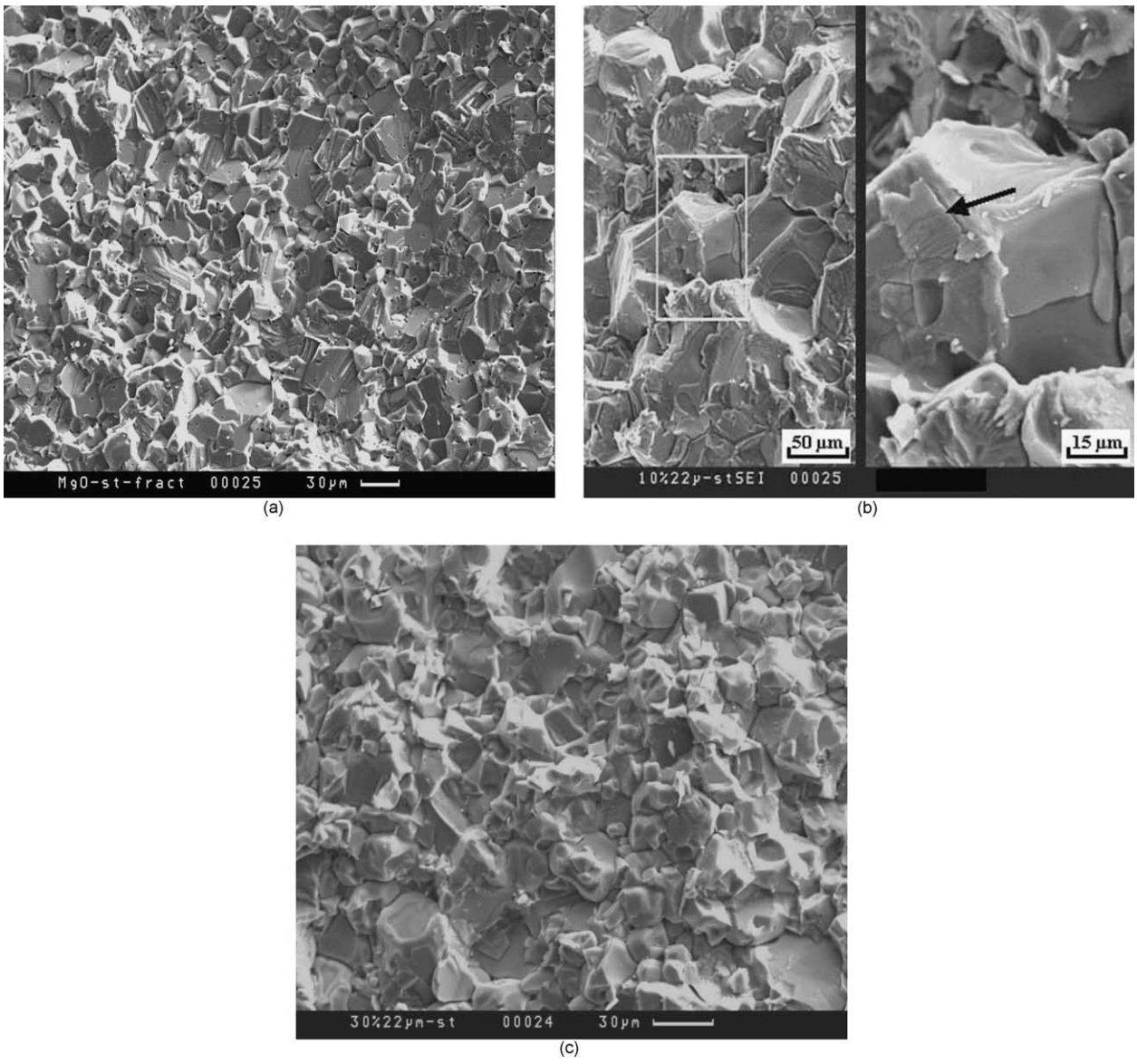

Fig. 2. a–c. Fracture surfaces of (a) pure magnesia, (b) 10%- and (c) 30%-containing 22 μm spinel-magnesia composites strength-tested *before* thermal shock.

mostly transgranular (through the grains) with clear grain cleavage. 10%-composites (Fig. 2b) still showed a large proportion of transgranular cracks in the fracture surfaces, like MgO—but the amount of intergranular fracture had increased: the occurrence of intergranular fracture is linked to the presence of spinel particles at the grain boundaries. The spinel particles were uniformly located at the grain boundaries and within the MgO grains, and there was no concentration of agglomerated spinel particles. For the 30%-composites the proportion of intergranular fracture increased markedly, with a few transgranular cracks (Fig. 2c).

3.3. Fractography after thermal shock

Fig. 3a–b show fracture surfaces after thermal shock from 800 °C. MgO showed a marked amount of transgranular fracture above the critical quench temperature, Fig. 3a—i.e. similar to before thermal shock. Fig. 3b shows that the 30%-composites had mostly intergranular fracture, after quenching from 800 °C. The higher the spinel content, the greater the amount of intergranular fracture.

A general summary of the fractography would be that the presence of increasing amounts of spinel causes the

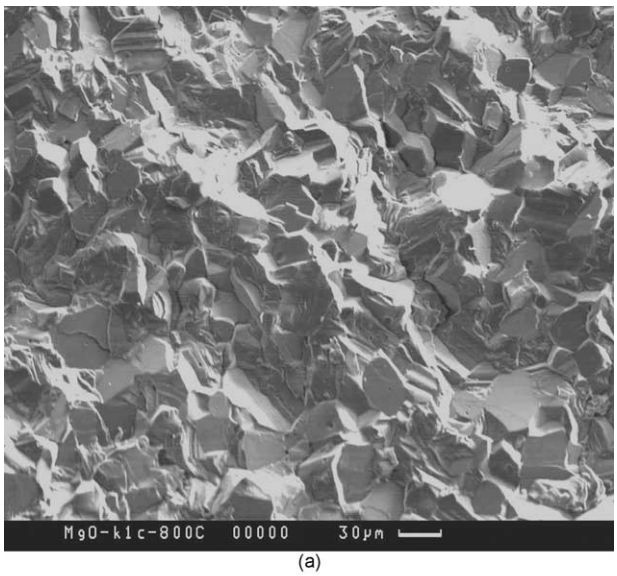

Fig. 3. a–b. Fracture surfaces of (a) pure magnesia and (b) 30%-containing 22 μm spinel–magnesia composites strength-tested *after* thermal shock.

fracture mode prior to thermal shock to change from predominantly transgranular to predominantly intergranular. After thermal shock from 800 °C, the fracture modes for any given material are predominantly unaltered from the pre-shock mode.

3.4. Work of fracture

Fig. 4 shows that spinel content is significantly effective in γ_{WOF} values in order to determine resistance to crack propagation and to further thermal shock damage. There was a marked increase in γ_{WOF}, by a factor of ~1.75, at 30% additions. The change in fracture path from transgranular to more intergranular fracture, with further spinel additions, is thought to be

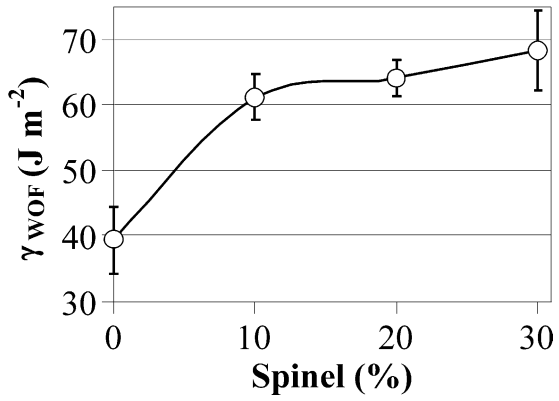

Fig. 4. Work-of-fracture (γ_{WOF}) as a function of spinel content.

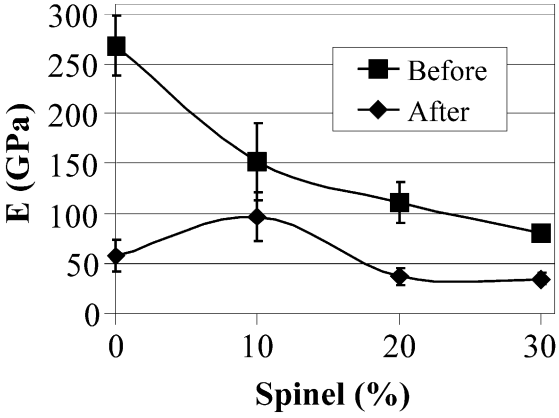

Fig. 5. Young's modulus (E) as a function of spinel content before and after thermal shock.

the main reason for the increase in γ_{WOF} energy required to propagate a crack completely through a specimen. It is possible that intergranular fracture along the smaller MgO grains, at higher spinel loading, requires much more energy for fracture than that for lower spinel loading, and this causes an increase in γ_{WOF} values.

3.5. Young's modulus

Fig. 5 shows the values of Young's modulus for MgO and the composite materials measured before and after thermal shock from 800 °C, where there is a dramatic drop for MgO, whereas the % drop for the composite materials is much smaller than that of MgO. As expected, the composite materials have a lower modulus than the pure MgO—not only is the modulus of spinel (238 GPa)[13,14] lower than that of MgO (260 GPa)[13,14] but the composites are micro-cracked as well, as detailed above.

3.6. Fracture toughness

Fig. 6 shows fracture toughness values (experimental and predicted) for MgO and the composite materials before and after thermal shock from 800 °C. The fracture

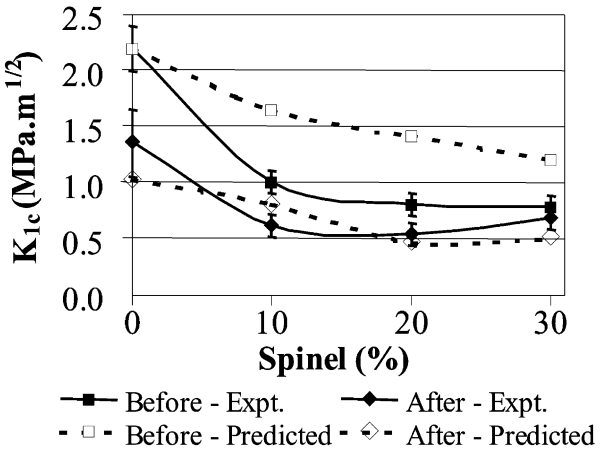

Fig. 6. Fracture toughness (K_{1c}) as a function of spinel content before and after thermal shock.

toughness of all materials drops before and after thermal shock: this drop can (largely) be accounted for by the associated drop in Young's modulus. The 'Before–Predicted' results are obtained by assuming that the fracture toughness of the composites is related to the fracture toughness of the MgO simply via the ratio of the square roots of the Young's modulus values [Eq. (6)].

3.6.1. Before thermal shock

The experimental composite toughness values are all less than that for the pure MgO—perhaps a surprising result in that one might expect crack deflection/crack bowing and other ceramic toughening mechanisms to be present. The 'Before–Predicted' values are calculated from the assumption that the lower Young's modulus of the composites is solely responsible for the drop in fracture toughness relative to the MgO, i.e.

$$\frac{K_{IC}(\text{Composite, Before})}{K_{IC}(\text{MgO, Before})} = \left(\frac{E(\text{Composite, Before})}{E(\text{MgO, Before})}\right)^{1/2} \quad (6)$$

It can be seen that this prediction is not particularly good—indicating there are also differences in the fracture surface energy between the composites and the pure MgO, presumably related to the change in fracture mode from transgranular to intergranular, referred to above, Section 3.2.

3.6.2. After thermal shock

For all four materials, there is a drop in fracture toughness following thermal shock. Again, predicted values are shown, assuming that the change in toughness is solely due to the drop in Young's modulus following thermal shock. In this case, the predictions are considerably closer to the experimental values—thus suggesting that there is little significant change in the fracture mode after shock.

3.7. Strength of materials

Fig. 7 shows the strength values (experimental and predicted) for MgO and the composite materials measured before and after thermal shock from 800 °C. The % drop in strength after shock for the pure MgO is much greater than that for the composites: indeed, the higher % spinel composites show no significant drop in strength following shock.

3.7.1. Before thermal shock

The strength of the composite materials is lower than that of the MgO. However, the observed composite strengths are generally lower (with the exception of the 10%-containing spinel) than would be expected simply from the drop in fracture toughness - suggesting a change in flaw size as well. In fact, the observed composite strengths can be predicted reasonably well by using the equation for the strength of a brittle material containing an inclusion of smaller thermal expansion coefficient. As shown by Swain,[46] when an inclusion of small thermal expansion coefficient is embedded in a material of higher thermal expansion coefficient, hoop tensile stresses are set up on cooling from the fabrication temperature. These stresses lead to the formation of radial cracks away from the particle-matrix interface, which may propagate catastrophically on further stressing. Swain shows that the fracture stress in such circumstances is given by

$$\sigma_f = \left(\frac{\beta K_{IC}^2}{ap^{1/2}}\right)^{2/3} \quad (7a)$$

where β is a constant ($\sim\pi/7$), K_{IC} is the fracture toughness, a is the particle radius, and p is the interface pressure at the particle–matrix interface, given by

$$p = \frac{(\alpha_p - \alpha_m)\Delta T}{(1-2\nu_p)/E_p + (1+\nu_m)/E_m} \quad (7b)$$

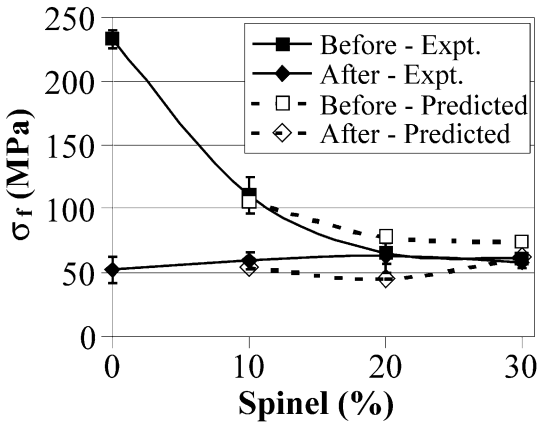

Fig. 7. Fracture strength (σ_f) as a function of spinel content before and after thermal shock.

where α_p, α_m are the thermal expansion coefficients of the particles and matrix, respectively and ν_p, ν_m and E_p, E_m are the Poisson's ratio and Young's modulus of the particle and matrix respectively. Assuming *local* values for the elastic constants, we have the table of values (Table 1):

Assuming a temperature drop of ~1100 °C (although the processing temperature is ~1650 °C, stress relaxation may occur in the MgO above ~1100 °C), an interface pressure of $p \sim 1.44$ GPa is predicted. Coupling this with the *global* fracture toughness values (as given in Fig. 6) and a particle radius of 11 μm, one predicts the strengths shown in Fig. 7.

3.7.2. After thermal shock

The strengths after thermal shock show a significant drop for the MgO, but a much less significant drop for the composites. The 20- and 30%-containing composites, in fact, show no loss of strength at all. Indeed, this is the reason why composite-type materials are used as refractories—they may not have particularly good strengths, but they do not lose significant amounts of strength following shock. Using Eq. (7a) allows one to predict the strengths of the composites following shock (assuming post-shock fracture toughness values): again, reasonable agreement with experiment is found.

3.7.3. Retained strength after thermal shock

Retained strength values, which are the strengths of bars after quenching relative to initial strengths, have been compared to evaluate thermal shock resistance of MgO and spinel composites, as a function of quench temperature (Table 2). Values for pure MgO were almost constant about <600 °C, but further increases in the quench temperature resulted in a sharp decrease in strength. The spinel composites for each spinel volume fraction had a higher retained strength than pure MgO from ~600 °C up to the maximum quench temperature used. In the weaker spinel composites, rather than fracture occurring catastrophically, any newly nucleated cracks and pre-existing cracks appeared to propagate only a short distance, suggesting that crack extension was small. Spinel composites were therefore more useful than pure MgO in terms of resistance to thermal shock damage and further loss of strength, where 30% 22 μm spinel composite showed the highest retained strength after thermal shock.

Table 1
Thermal expansion coefficient (α), Young's modulus (E) and Poisson's ratio (ν) of materials

Material	α (°C^{-1})	E (GPa)	ν
Spinel	7.6×10^{-6}	238	0.29
Magnesium oxide	13.5×10^{-6}	260	0.29

4. Conclusions

The higher the spinel content, the greater the crack length occurred due to the thermal expansion mismatch between MgO and spinel. At 30% spinel loading, a large number of interlinked cracks in the MgO matrix appeared, and the critical crack length increased significantly. Spinel particles mostly located along the grain boundaries leads to separation of grain boundaries and thereby a marked increase in the amount of intergranular fracture at fracture surfaces. Therefore, intergranular fracture along the smaller MgO grains, at higher spinel loading, requires much more energy for fracture than that for lower spinel loading, indicating higher γ_{WOF} values.

At room temperature, the fracture of MgO was mostly transgranular, and a large proportion of intergranular fracture was observed with increasing spinel content. After thermal shock, fracture surfaces of MgO showed that the extension of a large amount of combined intergranular fracture appeared with some transgranular fracture above the critical quench temperature, >600 °C. Spinel composites had mostly intergranular fracture, after quenching from 800 °C. The change in fracture path from transgranular to more intergranular fracture, with increasing spinel additions, is thought to be the main reason for the increase in γ_{WOF} energy. Pre-existing connected cracks appeared not to be able to propagate easily in the 20 and 30% spinel materials. For this reason, more energy was required to connect the cracks for propagation after thermal quenching. This change with spinel content may also be related to a slight increase in K_{1c} values at 30% for the composites quenched from 800 °C. Therefore, the cracks propagate only a short distance and become arrested. The composite

Table 2
Retained strengths of MgO and MgO–spinel composites, as a function of quench temperature (*: initial strength)

	Retained strength%		
ΔT/°C	MgO (233 MPa)*	10% 22 μm (110 MPa)*	30% 22 μm (60.5 MPa)*
200	100±16	85±17	100±6
400	100±17	75±17	98±9
600	48±40	61±7	93±6
800	22±4	54±3	92±5

containing 30% spinel in general shows the greatest resistance to crack propagation, and to further thermal shock damage.

Acknowledgements

Alcoa International (UK) Ltd. is thanked for supplies of materials. The contributions of the late Professor R.W. Davidge and Professor B. Rand are gratefully acknowledged. P. Bartha, S. Plint, and M.W. Roberts are also thanked for helpful discussions.

References

1. Maschio, R. D., Fabbri, B. and Fiori, C., Industrial applications of refractories containing magnesium aluminate spinel. *Industrial Ceramics*, 1988, **8**(3), 121–126.
2. Sanchez, J. A. R. and Toledo, O. D., New developments of magnesite-chrome brick and magnesite-spinel for cement rotary kilns higher thermal shock resistance and higher coating adherence. In *UNITECR 89*, 1989, pp. 968–979.
3. Gonsalves, G. E., Duarte, A. K. and Brant, P. O. R. C., Magnesia–spinel brick for cement rotary kilns. *Am. Ceram. Soc. Bull.*, 1993, **72**(2), 49–54.
4. Eusner, G. R. and Hubble, D. H., Technology of spinel-bonded periclase brick. *J. Am. Ceram. Soc.*, 1960, **43**(6), 292–296.
5. Sarkar, R., Das, S. K. and Banerjee, G., Effect of additives on the densification of reaction sintered and presynthesised spinels. *Ceram. Int.*, 2003, **29**, 55–59.
6. Moore, B., Frith, M. and Evans, D., Developments in basic refractories for cement kilns. *World Cement*, 1991, 5–12.
7. Sarkar, R., Das, S. K. and Banerjee, G., Effect of addition of Cr_2O_3 on the properties of reaction sintered $MgO–Al_2O_3$ spinels. *J. Eur. Ceram. Soc.*, 2002, **22**, 1243–1250.
8. Tabbert, W. and Klischat, H. J., Magnesia spinel bricks for the cement industry. In *Proceedings Beijing China Symposium*, 1992, pp. 424–430.
9. Laurich-McIntyre, S. E. and Bradt, R. C., Room temperature strengths of individual tabular alumina and sintered spinel grains (aggregates). In *UNITECR '93 Congress*, Sao Paulo, Brazil, 1993.
10. Bartha, P., Magnesia spinel bricks—properties, production and use. In *Refractory Raw Materials and High Performance Refractory Products, Proc. Int. Symp. Refractories*, ed. X. Zhong et al., 1989, pp. 661–674.
11. Klischat, H. J. and Bartha, P., Further development of magnesia spinel bricks with their own specific properties for lining the transition and sintering zones of rotary cement kilns. *World Cement, September*, 1992, 52–58.
12. Kimura, M., Yasuda, Y. and Nishio, H., Development of magnesia spinel bricks for rotary cement kilns in Japan. In *Proc. 26th Int. Col. Ref., Interceram Special Issue*, 1984, **33**, Aachen, Germany, 1983, pp. 344–376.
13. Shackelford, J. F., Alexander, W., Park, J. S., ed., *CRC Materials Science and Engineering Handbook*. CRC Press, Boca Raton, Florida, 1994.
14. Burnett, S. J., *Properties of Refractory Materials*. UKAEA Research Group Report, Harwell, 1969.
15. Soady, J. S. and Plint, S., A quantitative thermal shock approach to the development of magnesia–spinel refractories for the cement kiln. In *UNITECR '91*. Aachen, Germany, 1991, pp. 443–449.
16. Aksel, C., Rand, B., Riley, F. L. and Warren, P. D., Mechanical properties of magnesia-spinel composites. *J. Eur. Ceram. Soc.*, 2002, **22**(5), 745–754.
17. Aksel, C., Davidge, R. W., Warren, P. D. and Riley, F. L., Mechanical properties of model magnesia–spinel composite materials. In *Euro Ceramics V, Part 3, Extended Abstracts of the 5th Conference and Exhibition of the European Ceramic Society—Key Engineering Materials*, Versailles, France, 1997, **132–136**, pp. 1774–1777.
18. Aksel, C., Davidge, R. W., Knott, P. and Riley, F. L., Mechanical properties of magnesia-magnesium aluminate spinel composites. In *III. Ceramic Congress Proceedings Book*. Engineering Ceramics, Istanbul, Turkey, 1996, **2**, pp. 172–179.
19. Green, D. J., *An introduction to the mechanical properties of ceramics*. Cambridge University Press, Cambridge, 1998.
20. Hasselman, D. P. H., Unified theory of thermal shock fracture initiation and crack propagation in brittle ceramics. *J. Am. Ceram. Soc.*, 1969, **52**(11), 600–604.
21. Hasselman, D. P. H., Elastic energy at fracture and surface energy as design criteria for thermal shock. *J. Am. Ceram. Soc.*, 1963, **46**(11), 535–540.
22. Sack, R. A., Extension of Griffith's theory of rupture to three dimensions. *Proc. Physical Soc.*, London, **58**, 1946, pp. 729–736.
23. Aksel, C. and Warren, P. D., Thermal shock parameters [R, R''' and R''''] of magnesia–spinel composites. *J. Eur. Ceram. Soc.*, 2003, **23**(2), 301–308.
24. Aksel, C., Davidge, R. W., Warren, P. D. and Riley, F. L., Investigation of thermal shock resistance in model magnesia-spinel refractory materials. In *IV. Ceramic Congress, Proceedings Book, Part 1*, Eskişehir, Turkey, 1998, pp. 193–199.
25. Aksel, C., Thermal shock behaviour and mechanical properties of magnesia–spinel composites. PhD thesis, Department of Materials Engineering, University of Leeds, Leeds, UK, 1998.
26. Davidge, R. W. and Tappin, G., Thermal shock and fracture in ceramics. *J. Brit. Ceram. Soc.*, 1967, **66**, 405–422.
27. Morrell, R., *Handbook of properties of technical and engineering ceramics*, Part 1. Her Majesty's Stationery Office, London, 1985.
28. Watchman, J. B., *Mechanical properties of ceramics*. New York, 1996.
29. Davidge, R. W., *Mechanical behaviour of ceramics*. Cambridge University Press, Cambridge, 1979.
30. Aksel, C. and Riley, F. L., Young's modulus measurements of magnesia-spinel composites using load-deflection curves, sonic modulus, strain gauges and Rayleigh waves. *J. Eur. Ceram. Soc.*, 2003, **23**(16), 3089–3096.
31. Evans, R. M., Magnesia-alumina spinel raw materials production and preparation. *Am. Ceram. Soc. Bull.*, 1993, **72**(4), 59–63.
32. Wilson, D. R., Evans, R. M., Wadsworth, I. and Cawley, J., Properties and applications of sintered magnesia alumina spinels. In *UNITECR '93 CONGRESS*, Sao Paulo, Brazil, 1993, pp. 749–760.
33. Bradt, R. C., Fracture testing of refractories, past present and future. In *Proc. 2nd Int. Conf. on Refractories, Refractories '87*, Tokyo, **1**, 1987, pp. 61–68.
34. Aksel, C. and Warren, P. D., Work of fracture and fracture surface energy of magnesia–spinel composites. *Compos. Sci. Technol.*, 2003, **63**(10), 1433–1440.
35. Aksel, C. and Riley, F. L., Effect of particle size distribution of spinel on the mechanical properties and thermal shock performance of MgO–spinel composites. *J. Eur. Ceram. Soc.*, 2003, **23**(16), 3079–3087.
36. British Standard Testing of Engineering Ceramics, BS 7134 Section 1.2, 1989.
37. ASTM C1161-90, Standard Test Method for flexural strength of advanced ceramics at ambient temperature, *Annual Book of ASTM Standards*, 15.01, 1991, pp. 327–333.
38. ASTM D790M-86, Standard Test Methods for flexural properties of unreinforced and reinforced plastics and electrical insulating materials, *Annual Book of ASTM Standards*, 08.01, 1988, pp. 290–298.
39. Larson, D. R., Coppola, J. A., Hasselman, D. P. H. and Bradt, R. C., Fracture toughness and spalling behaviour of high-Al_2O_3 refractories. *J. Am. Ceram. Soc.*, 1974, **57**(10), 417–421.

40. ASTM E399-90, Standard Test Method for Plane–Strain Fracture Toughness of Metallic Materials, *Annual Book of ASTM Standards*, 03.01, 1991, pp. 485–515.
41. ASTM D5045-91, Standard Test Methods for plane-strain fracture toughness and strain energy release rate of plastic materials, *Annual Book of ASTM Standards*, 08.03, 1991, pp. 728–736.
42. Brown, W. F. and Srawley, J. E., *Plane strain crack toughness testing of high strength metallic materials*, ASTM Special Technical Publication, No: 410. 1967.
43. Davidge, R. W. and Tappin, G., The effective surface energy of brittle materials. *J. Mater. Sci.*, 1967, **3**, 165–173.
44. Coppola, J. A., Hasselman, D. P. H. and Bradt, R. C., On the measurement of the work-of-Fracture of refractories. *Am. Ceram. Soc. Bull.*, 1972, **17**, 578.
45. Mendelson, M. I., Average grain size in polycrystalline ceramics. *J. Am. Ceram. Soc.*, 1969, **52**(8), 443–446.
46. Swain, M., Nickel sulphide inclusions in glass: an example of microcracking induced by a volumetric phase change. *J. Mater. Sci.*, 1981, **16**, 151–158.